



JOURNAL OF COASTAL AND HYDRAULIC STRUCTURES

Vol. 5, 2025, 50

Validation of Lagrangian particle movement in CFD for simulating passive object transport over weirs

Linus Kaminski 101*, Carsten Thorenz 101, Roman Weichert 101, and Boris Lehmann 102

Abstract

Validated numerical models can facilitate the investigation of passive object transport over hydraulic structures. This study aims to validate the movement of Lagrangian particles in a numerical simulation using the two-phase OpenFOAM solver interFoam, modified to include particle tracking. A simplified weir overflow was modelled both numerically and physically, and the movement of spherical particles was analysed across three scenarios with varying tailwater levels. To evaluate the quality of this modelling approach, the validation focused on particle collisions immediately after weir passage, residence times within the study area, and upstream movements in recirculation zones such as the hydraulic jump and the water cushion between the weir and the nappe. These parameters were selected because the method is intended to contribute to a better assessment of downstream fish passage over weirs. Results from the numerical and laboratory models showed a high level of agreement. Collision counts and positions, as well as particle residence times and upstream movements, exhibited consistent trends across all three scenarios. The most significant deviation was observed in the number of particles entering the water cushion. This discrepancy is attributed to limitations of the Volume of Fluid (VOF) method, particularly the smearing of the air-water interface. Thus, when employing this methodology, it is essential to account for the inherent limitations of the applied numerical simulation approach. While a perfect replication of fish passage over a weir is not achievable, the method enables reliable qualitative comparisons across different configurations. It may therefore serve as a useful tool for evaluating hydraulic conditions relevant to fish passage.

- ¹ Federal Waterways Engineering and Research Institute (BAW), Karlsruhe, Germany
- ² Technical University of Darmstadt, Department of Civil and Environmental Engineering, Germany
- * linus.kaminski@baw.de

Research Article. **Submitted:** 29 April 2025. **Reviewed:** 23 Mai 2025. **Accepted** after double-anonymous review: 2 October 2025. **Published:** 27 October 2025.

DOI: 10.59490/jchs.2025.0050

Cite as: Kaminski, L.; Thorenz C.; Weichert R.; Lehmann B. (2025): Validation of Lagrangian particle movement in CFD for simulating passive object transport over weirs, *Journal of Coastal and Hydraulic Structures*, 5. https://doi.org/10.59490/jchs.2025.0050

The Journal of Coastal and Hydraulic Structures is a community-based, free, and open access journal for the dissemination of high-quality knowledge on the engineering science of coastal and hydraulic structures. This paper has been written and reviewed with care. However, the authors and the journal do not accept any liability which might arise from use of its contents. Copyright ©2025 the authors. This journal paper is published by TU Delft OPEN publishing under a CC-BY-4.0 license, which allows anyone to redistribute, mix and adapt, as long as credit is given to the authors.

ISSN: 2667-047X online

Keywords

OpenFOAM, lagrangian particle, CFD, downstream fish passage, weir, particle movement, particle tracking





1 Introduction

Computational Fluid Dynamics (CFD) is widely used in hydraulic engineering for the design and monitoring of hydraulic structures. The advantages of numerical modelling over laboratory models or field tests are cost effectiveness, flexibility and maximum control over boundary conditions and measurements (van Os et al., 2004). The simulation of passive object transport over hydraulic structures is relevant for a range of application, as e.g. downstream passage of fish (Greifzu et al., 2016; Romero-Gomez et al., 2024). However, reliable application requires in-depth knowledge and a thorough workflow validation (Thorenz et al., 2017). While the capabilities and limitations of two-phase (water and air) flow simulation are well understood (Argyropoulos & Markatos, 2015; Gisen et al., 2017; Naderi Rad, 2016), modelling ecological aspects such as the effect of passive migration of fish during downstream passage over weirs presents unique challenges.

For this purpose, a method is being tested at the Federal Waterways Engineering and Research Institute (BAW) in which passively migrating fish are represented in numerical simulations by using passive Lagrangian particles. In the numerical simulations, the particles are tracked and the hydromechanical parameters acting on them are analysed. The motivation for choosing this simplified approach lies in the high complexity and uncertainty involved in realistically modelling fish (Coutant et al., 2000; Jones et al., 2020). Morphological characteristics such as body shape and size vary greatly, and the behavioural responses of fish, especially during hydraulic passage events, remain insufficiently understood. Even if a realistic model could be developed for one particular species or life stage, it would likely not be transferable to other cases due to high variability between species, age groups, and individuals (Su et al., 2019; Bensing et al., 2022). Therefore, instead of aiming for high biological realism, a more generalised method was chosen, deliberately simplifying fish as neutrally buoyant spherical particles without active behaviour. This abstraction enables the simulation of a large number of particles and allows the evaluation of spatial and temporal patterns of movement in a statistically robust way. While this simplification cannot reproduce the exact behaviour of individual fish, it allows for a general assessment of potential fish paths and passage conditions. However, the particle-fluid interaction has not been validated to the same extent as the fluid flow itself.

A common way to increase confidence in a CFD method and increase its validity is the comparison with laboratory experiments, either supporting or refuting the hypothesis that the numerical model can reproduce reality (Taylor & Rumsey, 2021). An example of this approach is the work of Greifzu et al. (2016) in which point-particle dispersion models implemented in selected solvers of the CFD frameworks OpenFOAM and Ansys Fluent were compared with experimental data available in literature. Specifically, the authors evaluated particle dispersion in a turbulent channel flow using the Euler-Lagrange approach with RANS turbulence modelling. An underestimation of the particle dispersion by the modelling approach used in Ansys Fluent and an overestimation by the applied method in OpenFOAM were found. It should be noted that both Ansys Fluent and OpenFOAM are extensive simulation environments offering a wide range of models and configurations; the results therefore refer only to the specific model combinations tested in this study. Vollmari et al. (2016) compared experimental data with numerical models of a fluidised bed with spherical and nonspherical particles, obtaining good agreement for most particle types. Li and Li (2018) also found a good agreement between experimental data and numerical simulations using a combined volume-of-fluid (VOF) and discrete-elementmethod (DEM) solver of a gas-liquid-solid flow. The OpenFOAM particle solver DPMFoam was evaluated by Fernandes et al. (2018) through analytical, numerical and experimental comparisons, and found to be in agreement with results available in the literature. These studies demonstrate the relevance and potential of validating particle motion models through experimental setups. However, they also highlight that such validations are always specific to the modelling framework used. Therefore, a separate validation tailored to the specific numerical method applied in this study is essential to ensure its credibility and applicability.

Comparison with experimental or field data is also used to validate CFD approaches in the field of fish downstream migration, most notably in the context of turbine passage. Richmond et al. (2015) used field data of the passage through Kaplan turbines to find an acceptable reproduction of the nadir pressure distribution of a modelling approach. Similar autonomous sensors were also used by Benigni et al. (2021) to determine the conditions experienced by fish migrating through a Kaplan turbine. Additionally, live fish were externally instrumented with pressure sensors. These field data were compared with the lowest pressure of particle tracks from numerical simulations using the software package Ansys CFX, and good agreement of pressure changes was also observed. Similar experiments have also been carried out with a bulb turbine (Benigni et al., 2022). These studies, which focused on pressure changes, generally demonstrated that the







numerical methods used, based on Ansys CFX, are well suited for this application. A comparison of simulated Lagrangian spheres with autonomous sensor field data was performed by Romero-Gomez et al. (2017) with an acceptable agreement between simulated and observed data. The autonomous sensors used were able to track time histories of pressure, linear acceleration and rotational velocity, but not their spatial position during the passage, preventing a direct comparison of the trajectories. In addition, mean velocities and velocity fluctuations from the CFD model were compared with a scaleddown laboratory model. In comparing a CFD model with a laboratory model, Romero-Gomez et al. (2021) investigated the accuracy of a numerical method using Lagrangian neutrally buoyant inertial spheres moving in the subcritical flows past a circular cylinder. The proportion of particles colliding with the cylinder was almost identical in the numerical and the laboratory models. Another comprehensive model validation with experimental data for a modelling tool for fish passage through turbines was carried out by Singh et al. (2021). The CFD-predicted trajectories and collisions of small spherical and cylindrical particles were compared with laboratory experimental data. Furthermore, the method of particle collision detection was evaluated by comparing the impact velocity, collision time, velocity field and trajectory of a sphere with analytical values for a bouncing ball in the elastic collision. All predictions were in close agreement with the observed analytical and experimental results. These findings demonstrate that the use of Lagrangian particles can yield reliable results, supporting their suitability for modelling passive particle motion in hydraulically complex environments relevant to fish downstream migration.

The above studies address the two crucial questions regarding the validity of their methods, assuming the fluid field is correct: Is the simplification of fish acceptable? Is the numerical model able to simulate the particle motion correctly? This paper aims to answer the latter question for the CFD method described by Kaminski et al. (2024) with spherical, passively moving Lagrangian particles. The validity of the particle motion in the numerical model is examined by comparing numerical results with laboratory observations of spherical particles. In contrast to the cited studies, the present work focuses specifically on the intended application of the method for downstream passage over a weir. The processes relevant to this hydraulic setting are therefore placed at the centre of the analysis. Particular attention is given to transparently describing all forces and models implemented for particle motion. This is intended to allow comparison with other numerical approaches and facilitate reproducibility.

2 Methods

The movement of particles in a physical laboratory model is compared with the results of a numerical model. The models depict the same situation at the same scale. Since the study does not involve any geometric scaling, no scale effects are expected to influence the results. The hydraulic setup consists of a highly simplified aerated weir overflow into a stilling basin, which is bounded by an end sill. The flume has a width of 15 cm and the weir body has a height of 25 cm. A flow rate of 11 l/s was selected based on preliminary tests, which showed that this discharge results in a stable hydraulic condition that is not overly sensitive to minor fluctuations. This flow rate results in a headwater level of around 36.5 cm and therefore an overflow height of approximately 11.5 cm, both slightly depending on the height of the end sill. The stilling basin has a length of 150 cm, ending with an end sill. These specific dimensions were selected based on two main considerations: first, the model should be as large as possible within the spatial constraints of the laboratory flume; second, the observation area needed to be compact enough to ensure accurate optical tracking of the particles. It should be noted that the position of the end sill is not necessarily the position that would be chosen in reality. The primary function of the end sill is to maintain a certain tailwater level and to limit the test area downwards. The study examines three scenarios, each characterised by a different end sill height of 10 cm, 15 cm, and 20 cm, respectively, and consequently different water levels within the stilling basin. Figure 1 shows the observed section from the point of the particle addition to the end sill of the laboratory model and the numerical model. The models are flanked by an individual headwater and tailwater area. A full description of the two models is given in the following sections.





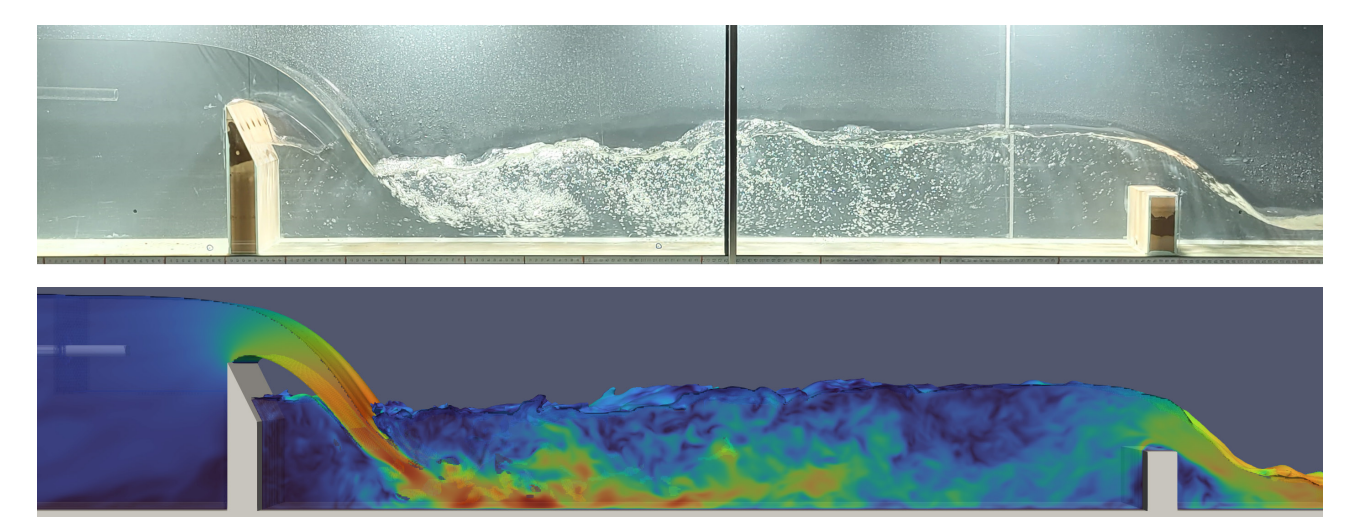


Figure 1: Comparison of the laboratory model (top) and the numerical model (bottom). The section from the particle addition on the left to the end sill on the right is shown. The low end sill variant is shown. The colours in the numerical model indicates flow velocity.

2.1 Physical laboratory model

The laboratory experiments were carried out in a recirculating water flume HM 163 manufactured by G.U.N.T. (G.U.N.T. Gerätebau GmbH, 2025) at the hydraulic engineering laboratory of the BAW in Karlsruhe, Germany. The flume has a length of 12.5 m, a height of 0.5 m and a width of 0.41 m. The width is reduced to 0.15 m by a built-in partition wall. The laboratory flume is shown in Figure 2. A centrifugal pump maintained a closed water circuit with a flow rate of 11 l/s, set and measured with an Endress + Hauser IDM Promag 53W1H (Endress + Hauser Group Services AG) with a maximum measurement error of \pm 2%. The inflow was conditioned by two aluminium honeycomb flow straighteners, one permanently installed in the inlet area, and a second one after the constriction to a width of 0.15 m. The observation section extended from the particle injection point to the end sill of the stylised stilling basin, starting 5 m downstream of the second honeycomb panel. The installations, the weir body and the end sill, were manufactured from polyurethane. To ensure an aerated nappe, holes were drilled in the downstream side of the weir and connected through the back wall to the atmosphere, allowing air to flow between the weir and the nappe. Particles were added through an injection tube with an outer diameter of 0.02 m and an inner diameter of 0.0127 m. The centre of the injection tube opening was placed 0.2 m in front of and 0.02 m above the weir crest (0.27 m above the flume bottom). A flow of 0.05 l/s through the tube resulted in a velocity of 0.4 m/s, similar to the surrounding velocity at this point.

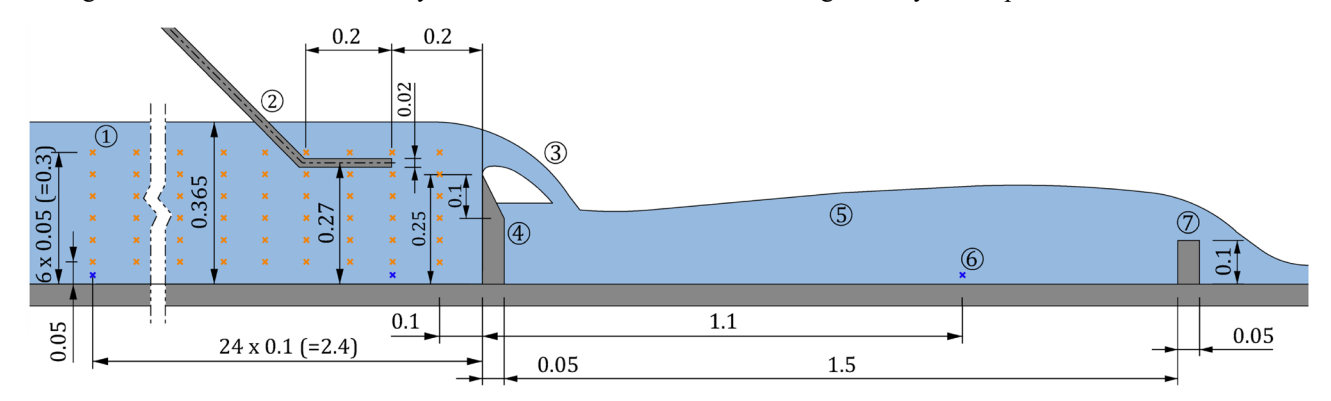


Figure 2: Schematic sketch of the laboratory model. (1) Positions of velocity measurements, (2) particle addition, (3) nappe, (4) weir, (5) stilling basin, (6) positions of water level measurements, (7) end sill.





2.1.1 Particles

Particles with a diameter of 10 mm were fabricated using the selective laser sintering technique. This resulted in spheres with a volume of 0.524 cm³. The material used was white Nylon 12 (PA 12) with a density of 0.95 g/cm³ and very low water absorption (3D Systems Inc.). To increase the density and achieve neutral buoyancy, 0.5 mm diameter holes were drilled in the particles and filled with lead. Slight variations in volume due to manufacturing imperfections made precise weight adjustment impossible. This was corrected by means of buoyancy tests in a water tank. An acceptable density, where the particles neither sink nor rise notably, was achieved for 45 spheres with an average weight of 0.513 g (standard deviation, SD = 0.050 g). The particles were dyed red to make them easier to identify, without any measurable change in density. The choice of a 10 mm diameter was based on the need to balance several practical constraints: the particles had to be as small as possible to be as close as possible to the also size constrained particles in the numerical model, while still allowing for sufficient manufacturing accuracy, density adjustment, and optical visibility during tracking.

2.1.2 Hydraulic boundary conditions

To achieve comparability between the laboratory and the numerical model, it is important to have detailed knowledge of the hydraulic conditions of the laboratory model. For this purpose, the water level in the headwater and the stilling basin and the velocity in the headwater were measured. The water level was calculated from the pressure measured at three points at the partition wall: At the x-position of the particle addition point, 2.2 m further upstream and in the stilling basin, 1.1 m from the weir crest. These points were connected to measuring pots via openings near the bottom of the partition wall, where water levels were recorded at a frequency of 40 Hz using SenSICK-UM18-2Hi ultrasonic probes for quasi-point distance measurements (SICK AG). Water level measurements were taken before the particle tests to determine the water levels, but also during the tests to detect any undesirable changes in flow and therefore water level. Flow velocity was measured prior to the particle trials in the headwater of the weir using a Nortek acoustic Doppler velocimeter (ADV). The ADV was mounted on a sled with a downward-facing probe. The mean flow velocity and the standard deviation of the flow velocity were recorded at 144 points along the centreline of the flume (y = 0). These are shown in Figure 2. Measurements were taken at heights of 0.05 m, 0.1 m, 0.15 m, 0.2 m, 0.25 m and 0.3 m above the bottom in 24 columns with 0.1 m between each column, starting from the weir. At each position the velocity information was determined from a sampling period of 120 s at 100 Hz. The transmission length was set to 1.8 mm and the cylindrical sampling volume to a diameter of 6.0 mm and a length of 7.0 mm. More information on these settings can be found in the user manual (Nortek AS, 2018).

2.1.3 Video recording

The movement of the released particles was recorded by a single camera. Accordingly, only the two-dimensional movement in the x-direction (flow direction) and z-direction was considered; the movement in the y-direction was neglected. The observation area was recorded with a Sony α 6300 with 100 fps and a resolution of 1920 x 1080 pixels (Sony Corporation, 2016). The camera was positioned slightly above the level of the flume bottom in the middle of the observation section, just between the weir and the end sill, at a distance of 5 m from the flume. The maximum error of the detected x-position at the edges of the observation section resulting from the camera position and the 0.15 m width of the flume, was ~0.012 m. Permanent LED video lighting was used from four different locations to achieve flicker-free illumination and visibility. The observation area was enclosed with stage molleton to avoid reflections on the flume's glass. In addition, a close-up of the area where the particles hit the ground was recorded with a GoPro Hero 12 Black at 100 fps and a resolution of 3840 x 2160 pixels (GoPro Inc., 2023). These images were used solely for visual comparison and validation of the automatic evaluation mimic.

2.1.4 Experimental procedure and post processing

A steady-state flow rate of 11 l/s was used for each end sill height scenario. Prior to starting the recording and adding particles, the model was run continuously for more than 10 minutes to stabilise the flow field. After the recording was started using a hand held start trigger, all the particles were added one at a time, at approximately one to two second intervals. Recording continued for 30 s after the last particle was injected, resulting in video sequences of approximately one to three minutes. In total, 38 to 43 runs per situation were recorded. The videos were then processed and the particle movements were tracked using Python version 3.11.9 (Python Software Foundation, 2024). The first stage of processing involved cropping the images to the required dimensions. Subsequently, the images were binarised. This was done using





the Python library OpenCV, version 4.10.0.84 (OpenCV.org, 2024). First, the colour model was changed to HSV (hue, saturation, value). A threshold filter was used to make pixels with an H-value of 164 to 180, an S-value of 100 to 255 and a V-value of 50 to 255 white, while all other pixels were made black. This process isolated pixels corresponding to particles from the background. The Python library Trackpy, version 0.6.2, was used to track the particles (Allan et al., 2024). Trackpy uses the Crocker-Grier algorithm to track blob-like features in sequential images (Crocker & Grier, 1996). However, due to occasional tracking gaps, approximately one quarter of the particle trajectories had to be manually reconstructed to create complete tracks. In this way, 1903 particle tracks were generated with a low end sill height of 10 cm, 1857 particle tracks with a medium end sill height of 15 cm and 1708 particle tracks with a high end sill height of 20 cm, each with a discernible origin and position information every 0.01 s. Nevertheless, some residual gaps still remain within the tracks.

2.2 Computational fluid dynamics

The comparative numerical simulations were performed using the open-source CFD library OpenFOAM (Jasak, 1996; Weller et al., 1998). The solver used is based on the widely used solver for two incompressible, isothermal immiscible fluids *interFoam* (Ubbink, 1997). This solver is based on the Volume of Fluid (VOF) method, an interface capturing technique used to track the interface between two immiscible fluids (Hirt & Nichols, 1981; Ubbink, 1997). The implementation by ESI Group in the version v2012 was used in this study.

The interFoam solver uses the Finite Volume Method (FVM) to discretise the governing equations of fluid motion. These include the Navier-Stokes equations for incompressible flow and additional transport equations for the phase fraction (Rusche, 2003). The VOF method represents the interface between the phases using a volume fraction field α , where $\alpha = 1$ indicates the presence of the primary phase (water), $\alpha = 0$ indicates the secondary phase (air), and $0 < \alpha < 1$ denotes the interface region. The governing equations solved by interFoam include the continuity equation (1), the momentum equation (2) and the phase fraction transport equation (3):

$$\nabla \cdot \boldsymbol{U} = 0 \tag{1}$$

$$\frac{\partial \rho U}{\partial t} + \nabla \cdot (\rho \boldsymbol{U} \boldsymbol{U}) = -\nabla p_{rgh} + \nabla \cdot \mu (\nabla \boldsymbol{U} + \nabla \boldsymbol{U}^T) + \rho \boldsymbol{g} + F$$
 (2)

$$\frac{\partial \alpha}{\partial t} + \nabla \cdot (\alpha \mathbf{U}) + \nabla \cdot [(1 - \alpha)\alpha \mathbf{U}_c] = 0 \tag{3}$$

U is the velocity vector, ρ is the density of the mixture of the two phases, t is time, p_{rgh} is a modified pressure that is used instead of p, μ is the dynamic viscosity of the fluid mixture and F is a continuum surface tension force model described by Brackbill et al. (1992). α is the volume fraction of the total volume that is occupied by water, where $0 \le \alpha \le 1$. Uc is an artificial compression velocity implemented in the *interFoam* solver to avoid the smearing of the interface between the two phases when solving the phase fraction transport equation with the FVM. The current implementation of the VOF method in *interFoam* is described in detail by Schulze (2018).

2.2.1 Lagrangian particles

In order to represent passively moving objects, the *interFoam* solver was extended to include Lagrangian particles. The decision not to use an existing particle solver such as *DPMFoam* or *MPPICFoam* was made for two reasons. Firstly, a multiphase solver is required to simulate the weir passage. Secondly, the aim was to maintain the simplicity of the method, which would be compromised by the introduction of complex models for heat transfer or particle-particle interaction. Since the approach aims at a general, species- and size-independent representation of fish, focusing on the particle trajectories and not elaborate collision mechanics, detailed particle properties and interactions that DEM allows were not necessary. The capabilities of the simpler Lagrangian particles were sufficient for this work. The *basicKinematicCloud*, a flexible and adaptable Lagrangian particle class, was included to simulate individual particles within the flow field. Although these particles allow feedback to the fluid field, i.e. a higher coupling order, this functionality was not used. One-way coupling was chosen to allow the addition of multiple particles with identical





properties in close proximity, or the inclusion of particles with different properties at the same location, without mutual interference, thus reducing the computational effort. Particles are strictly limited to spheres. The properties that can be adjusted are the diameter, the density and the patch interaction model. Particles can escape through a patch, rebound or stick to it. The rebound properties are defined by an elasticity and a restitution coefficient. Furthermore, the forces taken into account for the particle motion can be customised. According to Newton's second law of motion, the basic motion of a particle can be expressed as follows, specifying the most important forces:

$$m\frac{du}{dt} = \sum F_i = F_D + F_L + F_G + F_P + F_{VM} + F$$
(4)

where m is the mass of the particle, u is its velocity, and $\sum F_i$ is the sum of all the forces acting on the particle. The terms F_D , F_L , F_G , F_P , and F_{VM} refer to specific forces: F_D is the drag force, F_L is the lift force, F_G is the gravitational force, F_P is the force due to a local pressure gradient, and F_{VM} is the virtual mass or added mass force. The term F includes all other forces that are less significant than the aforementioned forces and were therefore not considered, including rotational or shear lift forces and thermophoretic forces. The force models used in this study are listed below:

The sphereDrag model was used to account for the drag force:

$$\boldsymbol{F_D} = \frac{3}{4} \frac{\mu_c \cdot C_D \cdot Re_p}{\rho_p \cdot d_p^2} \cdot -\hat{\mathbf{U}}_{rel} \tag{5}$$

where ρ_p is the particle density, μ_c is the dynamic viscosity of the carrier fluid at the cell occupied by the particle, d_p is the particle diameter, C_D is the particle drag coefficient, \hat{U}_{rel} is the unit vector of the relative velocity and Re_p is the particle Reynolds number, which is defined as follows:

$$Re_p = \frac{\rho_c \cdot |\boldsymbol{U_p}| \cdot d_p}{\mu_c} \tag{6}$$

where ρ_c is the density of the carrier fluid and U_p is the particle velocity relative to the carrier fluid. The SaffmanMeiLiftForce model was used to determine the lift force F_L . This model is based on the approach of Saffman (1965), extended by Mei (1992) to determine the lift coefficient C_L . It is implemented by the following equation:

$$C_L = \frac{3.0}{2\pi \cdot \sqrt{Re_{\omega} + \epsilon}} \cdot C_{ld} \tag{7}$$

where Re_{ω} is a modified Reynolds number (Equation (8)), ϵ is a small number to avoid dividing by zero, and C_{ld} is a preliminary lift coefficient (Equation (9)).

$$Re_{\omega} = \frac{\rho_p \cdot |\nabla \times \boldsymbol{U}_c| \cdot d_p^2}{\mu_c + \epsilon} \tag{8}$$

$$C_{ld} = \begin{cases} 6.46 \cdot f & \text{if } Re < 40\\ 6.46 \cdot 0.0524 \cdot \sqrt{\beta \cdot Re} & \text{if } Re \ge 40 \end{cases}$$

$$(9)$$

where ρ_p is the particle density, $|\nabla \times U_c|$ is the magnitude of the vorticity vector, and f and β are correction factors. The lift force F_L is then derived from the coefficient C_L according to the following equation:

$$\boldsymbol{F}_{L} = C_{L} \cdot \frac{1}{2} \rho_{c} \cdot A \cdot |\boldsymbol{U}_{\boldsymbol{p}}|^{2} \cdot \boldsymbol{e}_{L}$$
 (10)

where A is the characteristic area of the particle and e_L is the direction of the lift force, i.e. perpendicular to the direction of flow of the fluid. The gravity model applies a constant force on particles due to gravity and is calculated as





 $F_G = m_p \cdot g \cdot (1 - \rho_c / \rho_p)$, where m_p is the mass of the particle. The forces acting on the particles due to pressure gradients in the fluid are accounted for by the *pressureGradient* model:

$$\boldsymbol{F}_{\boldsymbol{p}} = -V_{\boldsymbol{p}} \cdot \nabla P \tag{11}$$

where V_p is the volume of the particle and ∇P is the pressure gradient. The final force model used is the *virtualMass* model, which takes into account the additional apparent mass that a particle appears to have when accelerated due to the need to accelerate the surrounding fluid. F_{VM} is calculated as follows, with a virtual mass coefficient $C_{VM} = 0.5$:

$$F_{VM} = C_{VM} \cdot \rho_c \cdot V_P \cdot \left(\frac{DU_c}{Dt} - \frac{DU_p}{Dt}\right) \tag{12}$$

2.2.2 Numerical model and simulations

The numerical model replicated the relevant section of the laboratory flume in which the laboratory experiments were carried out. The three-dimensional computational domain was defined as a rectangular box with a length of 6.0 m, a height of 1.0 m and a width of 0.15 m. The headwater had a total length of 2.4 m, followed by the weir structure, the stilling basin with a length of 1.5 m, the end sill and 2.0 m of tailwater. The hexahedral-dominated cells were refined based on a grid independence study, starting from a base cell length of 10 mm. All areas containing water were subjected to a single refinement step, resulting in a cell edge length of 5 mm. The observation area, including the particle addition, weir, and stilling basin, was subjected to two refinement steps, resulting in an edge length of 2.5 mm. This corresponds to a resolution of 60 cells across the width of the numerical model. No additional refinement was applied along the boundaries. The final product of this process were computational meshes with a total of 6.8 M (low end sill), 7.5 M (medium end sill) and 8.2 M (high end sill) cells.

The boundary conditions were defined to reproduce the laboratory model as closely as possible. The boundary conditions used are listed in Table 1. The inflow patch x_min is a special case. This boundary patch is primarily divided into two sections: the $inflow_air$ patch, above the water level, and the $inflow_water$ patch, which allows the inflow of water. The inflow-water patch is divided into four individual patches with the same boundary conditions but different settings. This in-house development allows for rotating areas with varying inflow velocities (Wagner, 2024). Originally developed to represent the outflow of a propeller or turbine, it has been used here to induce velocity fluctuations and turbulence. The selected settings are part of the model calibration which is described below.

Table 1: Boundary conditions of the numerical model and corresponding situation in the laboratory model for all boundary patches.

Boundary patch	Laboratory model	Boundary condition	
x_max	Open water/air outflow	Pressure inlet/outlet, fixed water table at $z = 0.0 \text{ m}$	
y_max	Glass pane, joint every 1.25 m Rough wall, Ks = 1·10-4 m		
y_min	PVC pane, joint every 1.75 m	Rough wall, $Ks = 1.10-4 \text{ m}$	
z_max	Open air inflow / outflow	Pressure inlet/outlet, fixed water table at $z = 0.0 \text{ m}$	
z_min	Stainless steel	Rough wall, $Ks = 1 \cdot 10-4 \text{ m}$	
weir	Polyurethane	Rough wall, $Ks = 1 \cdot 10-4 \text{ m}$	
end_sill	Polyurethane	Rough wall, $Ks = 1.10-4 \text{ m}$	
injection_tube	Acrylic glass	Rough wall, Ks = 1·10-4 m	
injection	Water inflow = 0.05 l/s	Fixed Inflow = 5e-5 m ³ /s, α = 1	
inflow_water	Water inflow = 11 1/s	Fixed propeller inflow = $1.1 \cdot 10-2 \text{ m}^3/\text{s}$, $\alpha = 1$	
inflow_air	Open air inflow / outflow	Pressure inlet/outlet, fixed water table at $z = 0.0 \text{ m}$	
aeration	Open air inflow / outflow	Pressure inlet/outlet, fixed water table at $z = 0.0$ m, $\alpha = 0$	





Reynolds-Averaged Navier-Stokes (RANS) turbulence modelling produces a time-averaged flow field without smallscale temporal variance, thereby smoothing streamlines and avoiding possible collisions. Therefore, large eddy simulation (LES) was used instead in order to resolve the small-scale fluctuations in fluid motion (Rodi, 2017). The k-equation model was used to model sub-grid scale eddies, while the larger high-energy turbulence structures were resolved directly (Yoshizawa, 1986). However, LES also requires an appropriate grid quality, which was validated in the grid independence study. For this purpose, four comparative simulations were carried out, each with a different refinement of the cells within the specified refinement range, covering the particle addition, the weir and the entire stilling basin. Grids with cell lengths of 1 cm, 0.5 cm, 0.25 cm and 0.125 cm were analysed. In each individual calculation, the discharge capacity of the weir was evaluated on the basis of the headwater level for the fixed discharge. Overall, only minor deviations were observed. Once a quasi-steady state was reached, the discrepancy in headwater level between a cell size of 0.25 cm and 0.125 cm, averaged over a 10 s interval, was less than 0.5 mm. The suitability of the grid for LES simulations was assessed using the Pope index (Pope, 2001). This criterion is based on the assumption that in order to obtain LES of acceptable quality, more than 80% of the total kinetic energy must be directly resolved in the entire flow field. Compliance with this criterion was checked by calculating the ratio of the directly calculated turbulent kinetic energy resolvedTKE (calculated from the modelled velocity fluctuations) to the total kinetic energy, the sum of resolvedTKE and k, the unresolved modelled turbulent kinetic energy. It is important to note that this method relies on the accuracy of the modelled turbulent kinetic energy k. As k is a result of the sub-grid scale turbulence model, this is not necessarily the true value but a commonly used approximation.

As shown in Figure 3, the criterion is already met in a considerable portion of the stilling basin, (blue areas) at a cell size of 1 cm. Only in the nappe and along the walls is less than 80% of the total kinetic energy resolved (red areas). This is still the case for a cell size of 0.5 cm. With a cell size of 0.25 cm, only the water-air interface of the nappe is red, indicating insufficient resolution to resolve the eddies in this shear zone. The results of the grid independence study indicated that a cell size of 0.25 cm was sufficient for the purpose of studying the turbulent flow field in the stilling basin and was therefore used in all subsequent simulations.

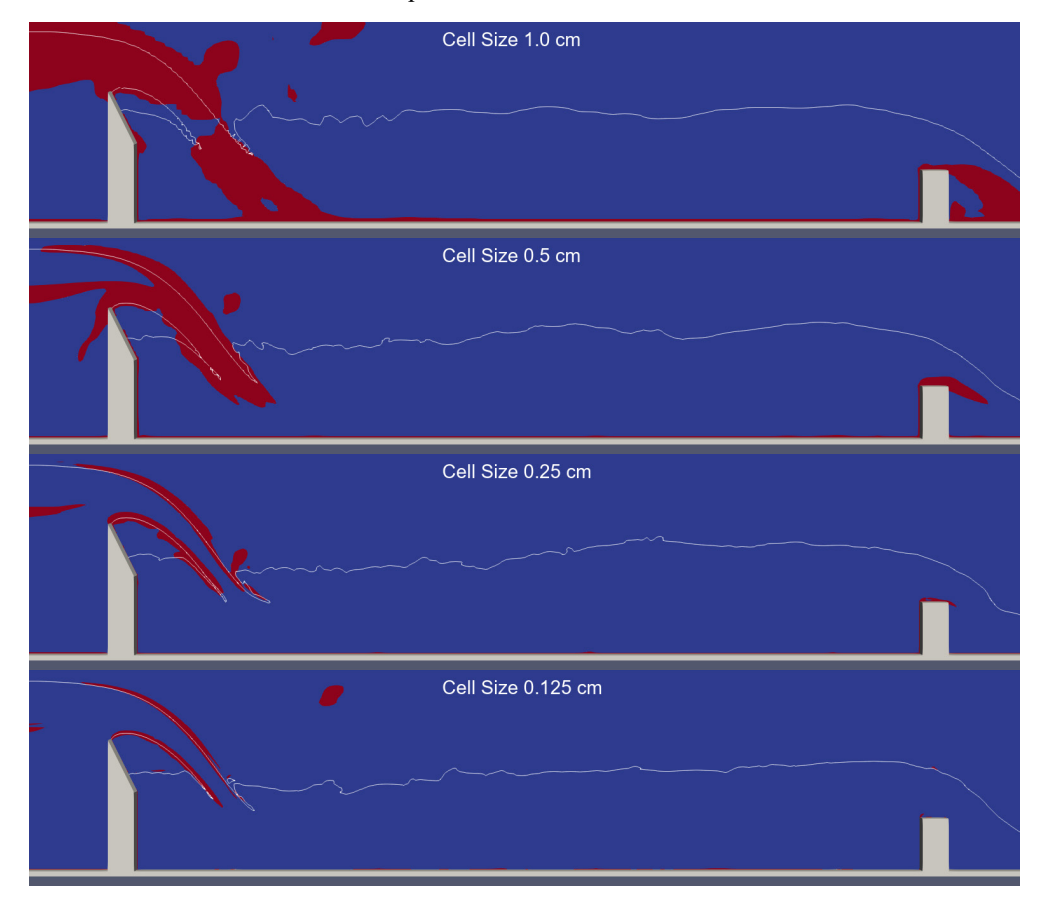


Figure 3: Pope index compliance of the different grid refinements. In the blue areas, the Pope index is fulfilled, as more than 80% of the total kinetic energy is resolved. This is not the case in the red areas. The white line shows the approximate water level.







In order to achieve a scenario as similar as possible to the laboratory model, the inflow was calibrated. As previously outlined, a custom propeller boundary condition, developed by Thorenz (personal communication) and described in more detail by Wagner (2024), was used to generate velocity variance and large-scale turbulence structures. The upstream model boundary of the numerical model was set to the position of the most upstream measurement profile in the laboratory model. At this point, the velocity profile of the numerical model was specified. Simulations of 30 variants with different boundary condition settings were carried out. Velocities and velocity variations were compared. Particular attention was paid to the profile at the point of particle addition. The number of inflow patches, the velocity amplitude, the rotational speed, the number of virtual rotor blades and the direction of rotation were varied. As in the laboratory model, measurements were taken at 100 Hz over 120 s. The best results in terms of mean velocities and velocity variances at the particle addition point profile were obtained with four inlet patches, a single rotor blade per patch, a relative velocity amplitude of 0.2 in the top and the bottom patches and 0.3 in the middle patches, and a rotational speed of 20 rpm. Using these settings, the mean velocity deviations from the laboratory model at the particle addition profile were 3% and the mean velocity variance deviations 16%. It is evident that a highly satisfactory alignment of the hydraulic situation was achieved. The mean headwater level recorded during the tests was 362.9 mm in the laboratory model and 363.9 mm in the numerical model. The discharge coefficient calculated from this differed by only 1.3%.

Preliminary simulations were used to reach a quasi-stationary state. Once this had been achieved, an additional 100 s were simulated to generate different initial conditions for the particle simulations. Every second full second between 21 s and 99 s was used as the initial condition for a particle simulation. The particles were initialised in the first time step at five points where they could emerge from the injection tube: Exactly at the centre of the tube and three millimetres in the positive and negative y and z directions. Due to numerical constraints, the particles must be considerably smaller than the cells of the mesh. A particle diameter of 0.1 cm was therefore chosen. Due to the size difference between the numerical and laboratory model particles, it was necessary to scale the numerical particle density to achieve the same terminal velocity as in the laboratory model, thus reflecting the imperfections of the manufacturing process. To do this, the descent or ascent velocity of each particle, depending on whether the actual density was slightly above or below that of water, was measured in a cylindrical container with a height of 50 cm and a diameter of 15 cm. The density of the numerical particles was recalibrated to reproduce the observed behaviour in an even distribution. Consequently, particles with densities of 0.85 g/cm³, 1.00 g/cm³, 1.10 g/cm³, 1.15 g/cm³, 1.20 g/cm³, 1.23 g/cm³, 1.27 g/cm³, 1.30 g/cm³, 1.33 g/cm³ and 1.37 g/cm³ were initialised at each of the five starting points. The particles were given an initial velocity of 0.4 m/s, corresponding to the water velocity in the injection tube. Following this pattern, 40 simulations were run with 50 particles each for each of the three situations, resulting in 2000 particle trajectories per situation.

2.3 Analysis and comparison

In order to compare the particle behaviour in the numerical model and the laboratory model, the following factors are taken into account: The number and positions of collisions, the time spent in the stilling basin and the number of particles entering areas of counter-flow, i.e. the water cushion between the weir and the nappe and the hydraulic jump backflow. Collisions are a major contributor to fish injury during downstream migration and therefore need to be modelled accurately. In general, however, the selection of the criteria for comparison is based on an effective evaluation of particle movement without making a direct reference to fish.

Based on the number of particle tracks N, the proportion of particles exhibiting a specific behaviour is expected to fall within the range $P \pm e$, where P is the true proportion derived from observations and e is the margin of error. The margin of error, based on a 95% confidence interval (95% CI results in Z = 1.96), is calculated using the following equation:

$$e = Z \cdot \sqrt{\frac{P(1-P)}{N}} \tag{13}$$

However, a similarity of behaviour goes beyond the assessment of significant differences. Even in the presence of a significant difference, a similarity of results may permit the use of qualitative comparisons. For this reason, an engineering judgement is also made.







The particle position was recorded every 0.01 s in both models. Due to this discontinuous particle tracking and small inaccuracies in the exact position determination in the laboratory model due to distortion and calculation of the particle centre point, it proved difficult to judge whether or not a collision had occurred. Consequently, three categories were defined: "No contact", where the particle clearly did not come into contact with the wall, "Probable contact", where a particle came close to the wall but it was ambiguous whether the particle and wall touched, and "Collision", where there was an unambiguous collision. An automatic detection model was developed and calibrated by watching the videos of the particle tracks. This model was used in the same way for the collision detection in both the numerical and the laboratory models. Based on the video analysis, collisions were detected within a range of 0.15 m to 0.55 m downstream of the weir.

If a particle centre did not come closer to the wall than 1 cm (the diameter of a sphere in the laboratory model), a "No contact" was assigned. If a particle centre came closer to a wall than 1 cm, a "Collision" was assigned if the average velocity perpendicular to the wall was greater than 0.3 m/s in at least one of the last five time steps and it started moving upwards again, otherwise a "Probable contact" was assigned. Exclusively the primary collisions immediately after the weir passage were considered, as these in particular must be accurately modelled by the method. Further collisions during passage through the stilling basin or with the end sill are less important, because it is assumed that fish will eventually resume active swimming behaviour to avoid collisions. These further collisions are therefore ignored.

The mean and the median of the residence times in the stilling basin were calculated from the time of passing the weir crest (x > 0.4 m) to the point in time of passing the upper edge of the end sill (x > 1.95 m). Movements in the negative x-direction, against the main flow, were classified according to the position in "Water cushion" between weir and nappe and "Hydraulic jump". The number of particles that entered one of these areas and moved at least 1 cm against the main flow direction was recorded, as was the mean distance travelled in the negative x-direction. In the following chapter the numerical model is referred to as "N" and the laboratory model "L".

3 Results

In the laboratory model, 1903, 1857, and 1708 particle tracks were recorded for the low, medium, and high end sill cases, respectively, while 2000 tracks were analysed for each scenario in the numerical model. Figure 4 shows the trajectories of 40 particles, corresponding to approximately every 50th particle, for all six cases. This is a random selection to observe the general behaviour of the particles. The evaluated motion patterns can also be clearly seen. After the nappe, collisions with the bottom occur. Rotational motions can be seen in the water cushion between the nappe and the weir and in the hydraulic jump. The general picture is very similar in all three situations. The limited number of particles does not allow for a detailed comparison; this is done in the following sections for the whole of the particle trajectories.





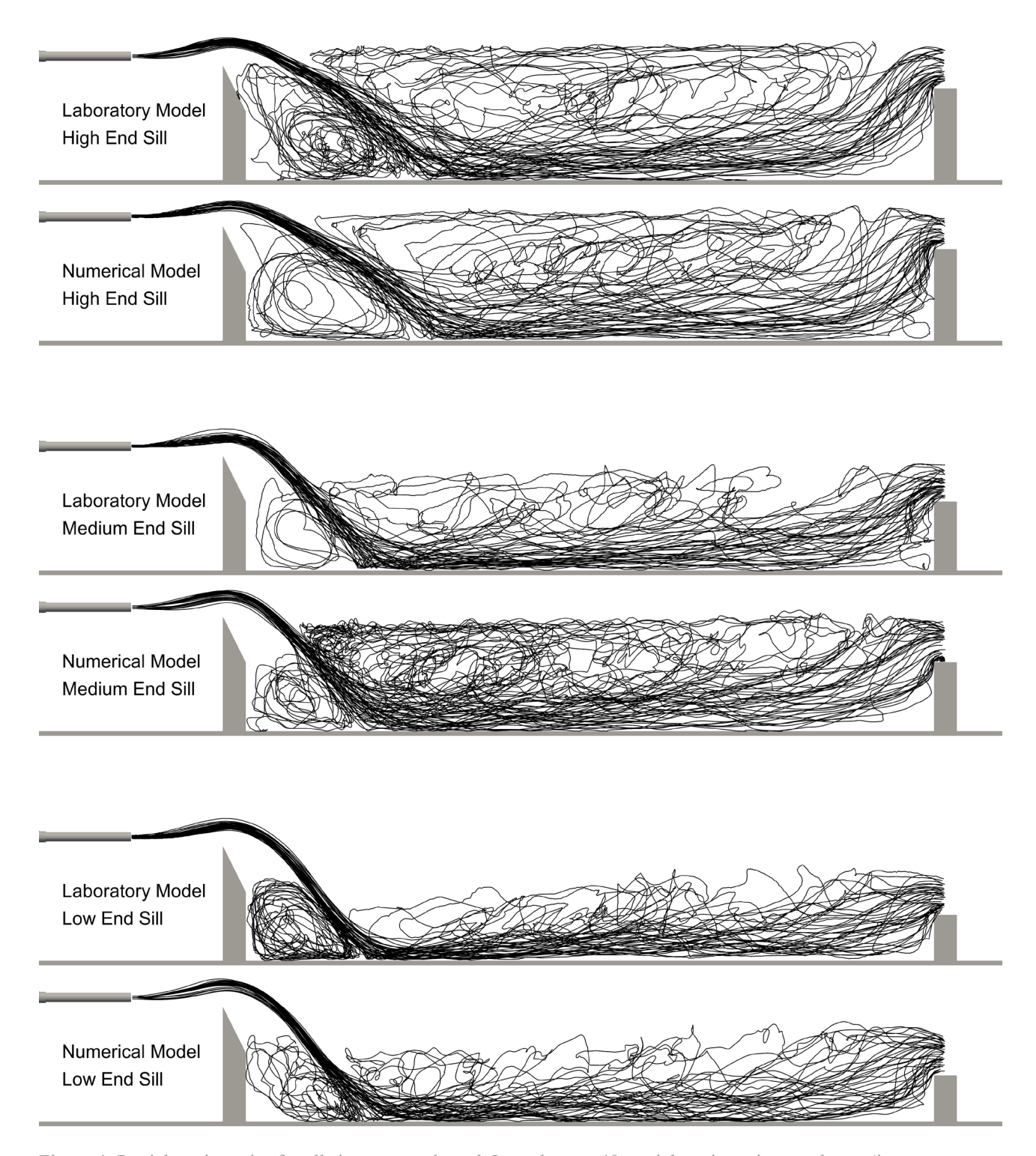


Figure 4: Particle trajectories for all six cases evaluated. In each case, 40 particle trajectories are shown (i.e. approximately every 50th particle) from the particle addition position to the end sill.

3.1 Collisions

The results of the collision tracking are shown in Figure 5. The overall trend observed in both models is consistent. As the tailwater level increases, the frequency of clear collisions decreases, while the proportion of particles without bottom contact increases. The number of probable collisions remains relatively constant for all scenarios tested. The agreement between the numerical model and the laboratory model is high. The underlying trends are identical for all three scenarios, and the observed proportions of clear collisions, probable contacts and particles with no contact are consistently





close. The mean discrepancy between the two models is 2.6 percentage points in relation to the total number of particles, with a maximum divergence of 8.9 percentage points. Nevertheless, there are some differences between the two models. The occurrence rate of "no contact" is consistently higher in the numerical model in all three scenarios, while "clear collisions" are consistently less frequent.

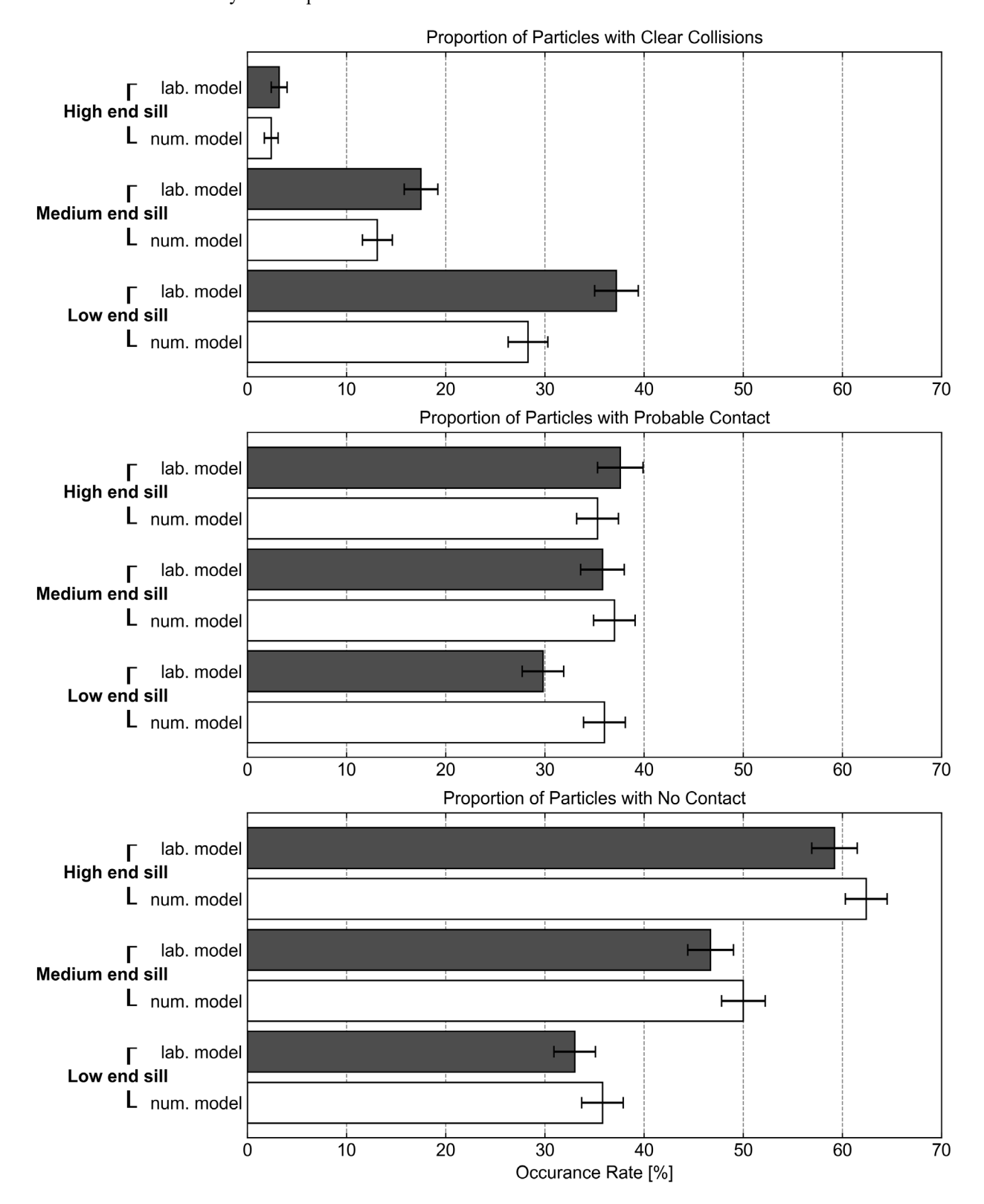


Figure 5: Results of the collision evaluation. Divided into particles with clear collisions, possible contacts and no contact with the bottom for the low, medium and high tailwater situations respectively. Error bars indicate the 95% confidence intervals.







In addition to the number of collisions, their positions were also compared. Figure 6 shows the positions of all clear collisions in the laboratory model on the left and in the numerical model on the right. It is noteworthy that the distance of the collisions to the weir initially decreases when moving from the low to the medium tailwater level, but is then highest at the high tailwater level. This trend is consistent for both models. The mean positions of the collisions are within 1 cm (L = 0.8 cm, M = 1.0 cm, H = 0.6 cm). The shape of the distribution is also similar in both models. An exception to the general pattern is the high tailwater situation. In this case, the sample size is relatively limited due to the low number of collisions, which is 47 and 55, respectively.

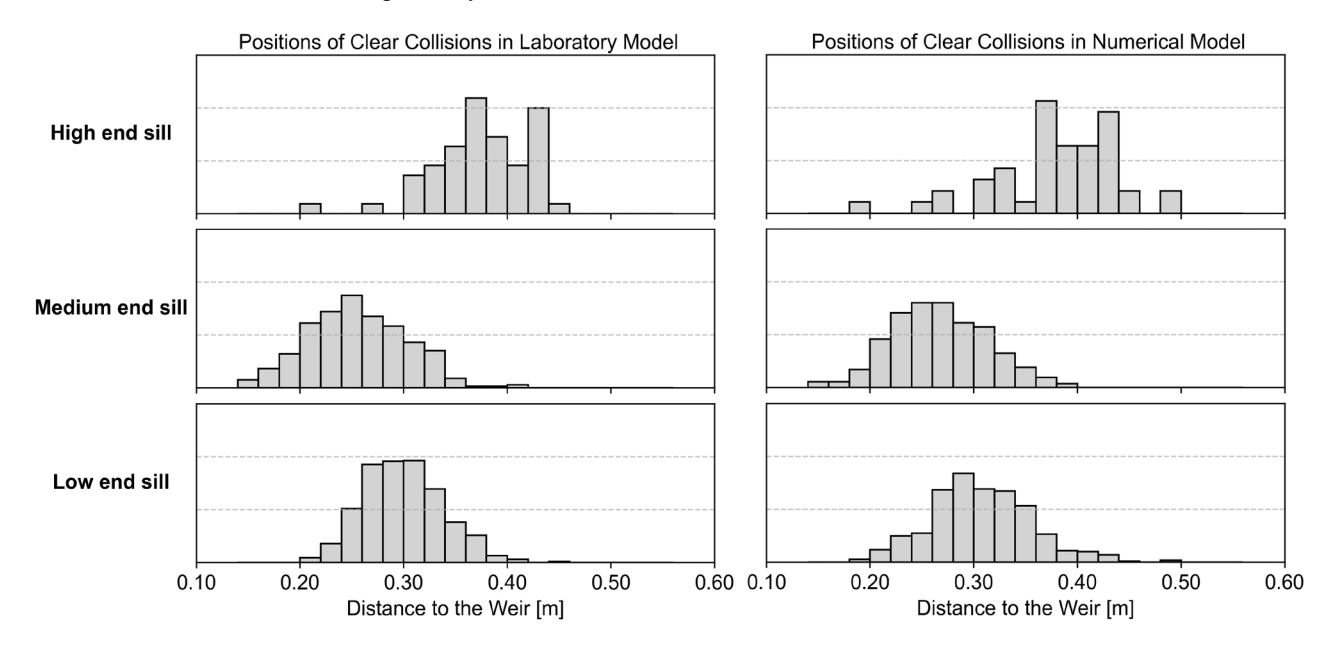


Figure 6: Locations of observed collisions.

3.2 Upstream movement

There were two areas where particles could enter a counter flow and move upstream: The water cushion between the weir and the nappe and the hydraulic jump. Accordingly, particles moving upstream were counted separately for both areas. Figure 7 shows the proportions of particles that moved upstream for at least 0.01 m in the water cushion or the hydraulic jump, or did not move upstream at all. As a single particle can enter both areas of upstream movement, the proportions do not necessarily add up to 100%. The main difference between the models is the proportion of particles showing upward movement within the water cushion. This behaviour was less frequent in the numerical model, especially in the low tailwater case. Consequently, the proportion of particles that did not move upstream was higher in the numerical model compared to the laboratory model. The proportions of particles moving upstream in the hydraulic jump were very similar. The only exception was observed in the low end sill situation. In this case, the number in the laboratory model was considerably higher than in all other cases. The pattern of upward movement is consistent in both models. As the tailwater level rises, the upward movement in the water cushion increases, while that in the hydraulic jump is the highest for the low end sill, but relatively stable.





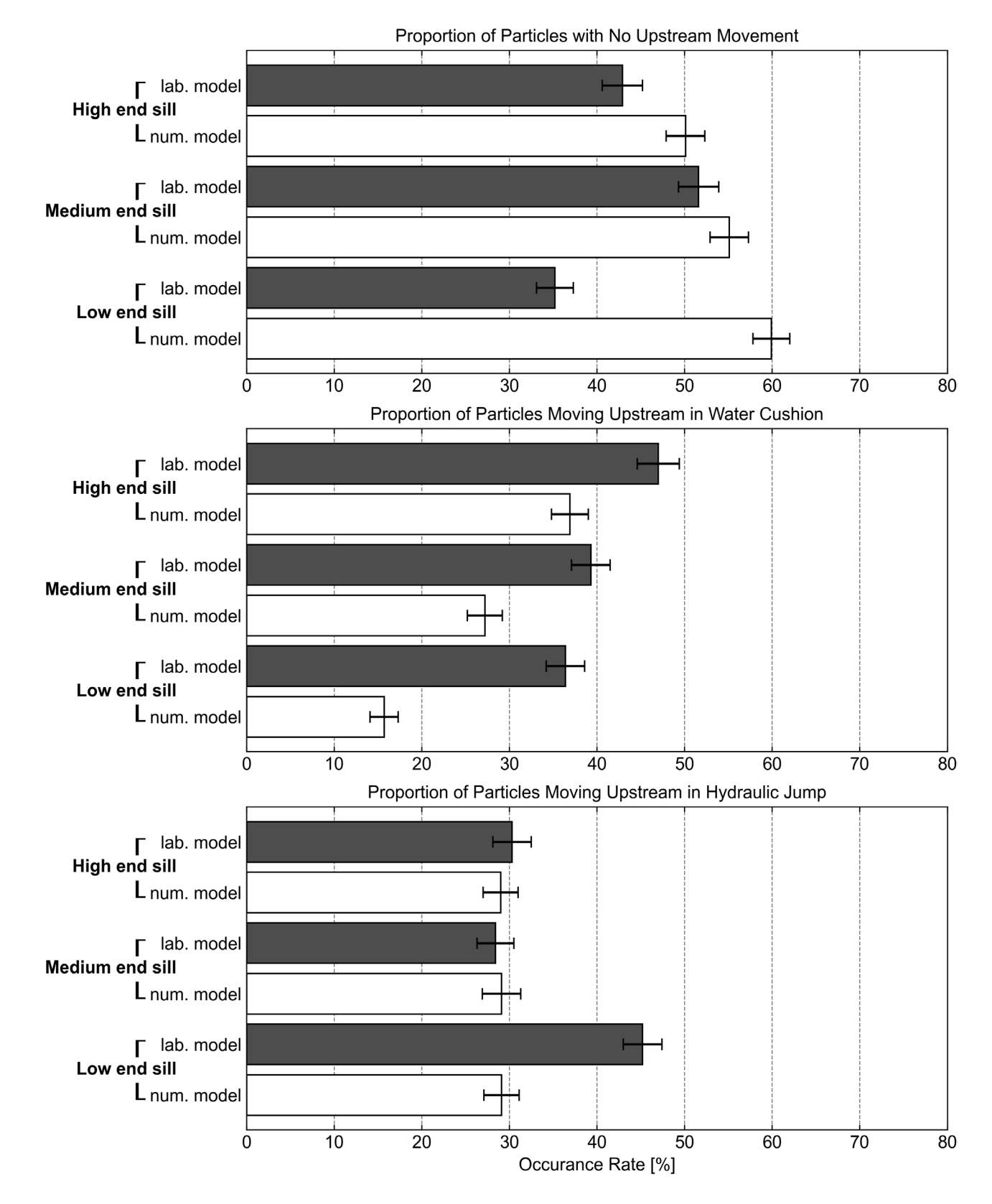


Figure 7: Results of the upstream movement assessment. Divided into particles with no upstream movement and upstream movement in the water cushion and the hydraulic jump for the situations with low, medium and high tailwater level respectively. Error bars indicate the 95% confidence intervals.





In addition to the occurrence of upstream movement, the distance travelled upstream was also analysed. Figure 8 shows the cumulative upstream distance travelled by each particle in the water cushion and in the hydraulic jump. In general, it can be seen that the distances travelled upstream in the water cushion are considerably longer, with medians of well over 0.2 m and up to almost 0.5 m. This is due to the fact, that particles can be trapped in the water cushion in a rotating motion behind the weir for an extended period of time and thus accumulate a considerable travel distance. Overall, the distances travelled in the water cushion increase with a higher tailwater levels in both models. This is not necessarily the case for the upstream movement in the hydraulic jump.

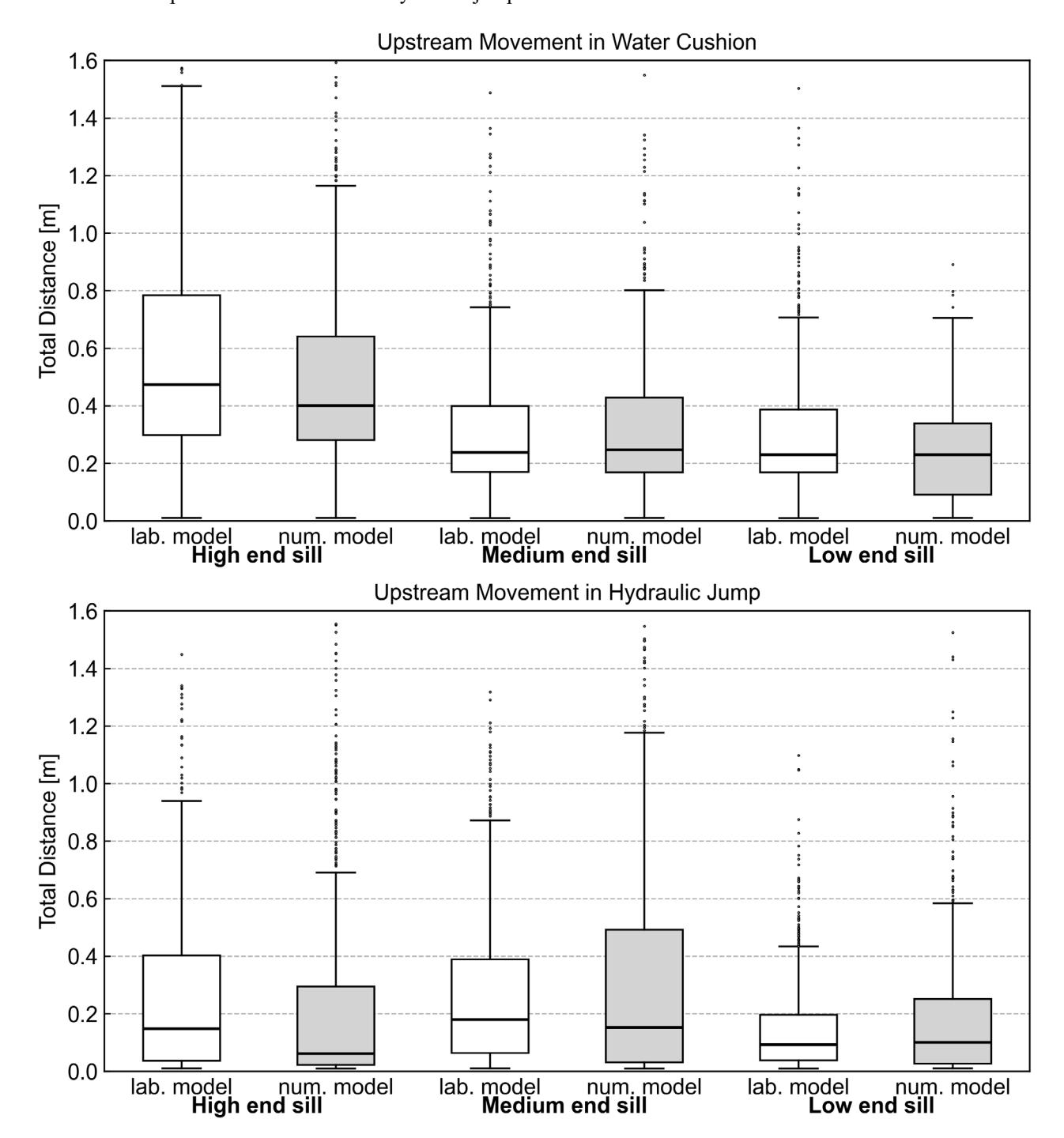


Figure 8: Total distance travelled upstream in [m] for each particle.





3.3 Residence time

Given the significant differences observed between the considered variants in terms of upstream movement, and the strong dependence of the residence time in the relevant area on this factor, an adjustment was made to the evaluation of the residence time: In addition to the residence time of all particles, the residence time of particles without upstream movement and the residence time of particles with upstream movement were analysed separately. Table 2 shows the mean, median, minimum, and maximum values as well as the standard deviation of these three groups.

The majority of the particles traversed the test area in a relatively short period of time, typically within a few seconds. However, some particles exhibited a prolonged residence time in the backflow areas, resulting in an overall residence time considerably longer than the average. In all cases, the mean value is significantly higher than the median due to the influence of these outliers. This effect was observed more frequently when the tailwater level was higher, which can be attributed to a lower water exchange rate due to a larger volume of water at the same flow rate in these cases. Furthermore, the maximum values showed an increase in relation to a higher tailwater level. As a result, the 20 s simulation time in the numerical model was not sufficient for all particles to reach the end of the study area. This implies that in these cases, the actual maximum residence times remain unknown and the averages are also subject to small alterations. However, this does not affect the median values. For this reason, and due to the significant impact of outliers on the mean values, the analysis focuses primarily on the median values.

Overall, the residence times in the numerical model are shorter than in the laboratory model, except for particles with upstream movement. However, the general trend is the same in both models: As the tailwater level rises, the residence time of the particles with and without upward movement increases. The increase is comparable in both models and is significantly lower for the particles without upward movement (L = 9%, N = 9%) than for the particles with upward movement (L = 36%, N = 97%).

Table 2: Residence times in the observation area for all particles and divided into particles with and without upstream movement. SD, Standard Deviation.

		Mean	Median	Min.	Max.	SD
	All particles	6.30	4.50	1.75	43.50	4.97
High end sill, lab. model	No upstream	2.62	2.45	1.75	7.70	0.66
	Only upstream	9.07	8.04	1.88	43.50	5.02
	All particles	4.36	3.32	1.46	28.98	3.03
Medium end sill, lab. model	No upstream	2.34	2.17	1.46	6.13	0.62
	Only upstream	5.94	5.03	1.89	28.98	3.23
	All particles	4.14	3.38	1.24	25.30	2.59
Low end sill, lab. model	No upstream	2.13	2.05	1.24	4.79	0.51
	Only upstream	5.12	4.46	1.48	25.30	2.63
	All particles	9.04	5.28	1.26	20*	7.70
High end sill, num. model	No upstream	4.64	2.06	1.26	20*	5.90
	Only upstream	13.45	15.23	1.59	20*	6.73
	All particles	5.09	2.99	1.21	20*	4.79
Medium end, sill num. model	No upstream	2.78	1.93	1.21	20*	2.64
	Only upstream	7.99	6.16	1.68	20*	5.30
	All particles	3.96	2.19	1.05	20*	4.52
Low end sill, num. model	No upstream	2.01	1.72	1.05	14.10	1.07
	Only upstream	6.58	4.22	1.51	20*	5.72

^{*}Duration set manually, as some particles did not leave the observation area within the simulation time of 20 s.





4 Discussion

In order to make a meaningful comparison of the particle trajectories, it is first necessary to determine the degree of agreement between the numerical model and the laboratory model, and to identify any discrepancies between the two. In general, subsequent measurements demonstrated that the models exhibited a satisfactory degree of geometric similarity. The upstream boundary condition of the numerical model was calibrated to match the situations measured in the laboratory model in the headwater area, resulting in a highly satisfactory agreement between the mean velocities and the velocity variance. The water levels also showed a high degree of agreement. The aeration of the nappe was observed to function as intended in both models, as was the addition of particles. On average, the particle velocities in the numerical model and the laboratory model were found to be highly similar in the area of the weir crest. As shown for the low end sill situation in Figure 1, this gives a highly similar picture of the flow field in the laboratory model and the numerical model.

A more detailed examination reveals that the situation of the particle movements is not entirely the same. Although the mean velocities of the particles as they cross the weir crest are equivalent, the laboratory model exhibits a significantly higher variance. In the numerical model the particles were initialised with a fixed velocity of 0.4 m/s in the positive x-direction. This corresponds to the average velocity observed in the injection tube in the laboratory model. However, the actual velocity of the particles in the laboratory model is influenced by both velocity fluctuations and wall contact of the particles in the tube. Another difference between the models is the size of the particles. In the laboratory model, the spheres had to be 1 cm in diameter to achieve the appropriate density and allow tracking. However, the numerical method requires particle diameters considerably smaller than the cell size. For the 0.25 cm cell size used, a particle diameter of 0.1 cm was chosen. However, the actual difference between the particles in terms of shape and density is unknown. Due to the small size of the objects, even minimal variations in the printing process lead to substantial deviations in volume and density. Trying to make up for this, the density was manually adjusted to 1 g/cm³, but only the mass and not the density of the objects could be monitored. In the numerical model, the given density is always exactly maintained, there are no deviations. An attempt has been made to compensate for this by using particles with different densities, resulting in the same descent or ascent velocities.

Another difference, which has a substantial effect on the movement of the particles, is the exchange of fluid and momentum between the nappe and the water cushion. The momentum of the overflow jet gives rise to a steady rotational motion of the water cushion. An underestimation of the momentum exchange in the shear zone is caused by the VoF method used in the numerical simulation. Treating air and water as a mixture described by a phase volume fraction leads to the problem of numerical diffusion, which causes a smearing of the initially sharp interface. This leads to an exaggerated downwards transport of air at the nappe interface into the water body. This phenomenon leads to the formation of a separating layer of air between the nappe and the water cushion situated between the nappe and the weir body. This in turn results in a reduction in the momentum exchange between the water cushion and the nappe, which is not consistent with the laboratory model. In the numerical model, as long as the weir is aerated, the separation of the water bodies reduces the magnitude of this effect, resulting in a lack of the large-scale rotational motion, as shown in Figure 9. This also reduces the mass transfer between the nappe and the water cushion. This effect is only present in the low tailwater situation. With the higher tailwater level, the weir is no longer aerated in the medium and high end sill situations. For all flow situations, the exchange of momentum between the nappe and the water cushion is underestimated in the numerical model due to an insufficient grid resolution of the shear zone. In Figure 3 we can see that the shear zone is indicated as "not sufficiently resolved for LES". As a consequence, turbulent eddies cannot develop sufficiently and the transport of both momentum and particles into the water cushion is underestimated.

Furthermore, the tracking process in the laboratory model introduces an additional element of uncertainty. Discrepancies between the detected position and the actual position may arise due to the angle of view of the camera and the depth of the flume. There is also the possibility that the centre of the detected object may not align precisely with the actual centre of the particle. In contrast, the numerical model consistently gives the exact position of the particle centre. In the following sections, collision, upstream movement and residence time are discussed, with particular consideration of the model deviations that have been identified.





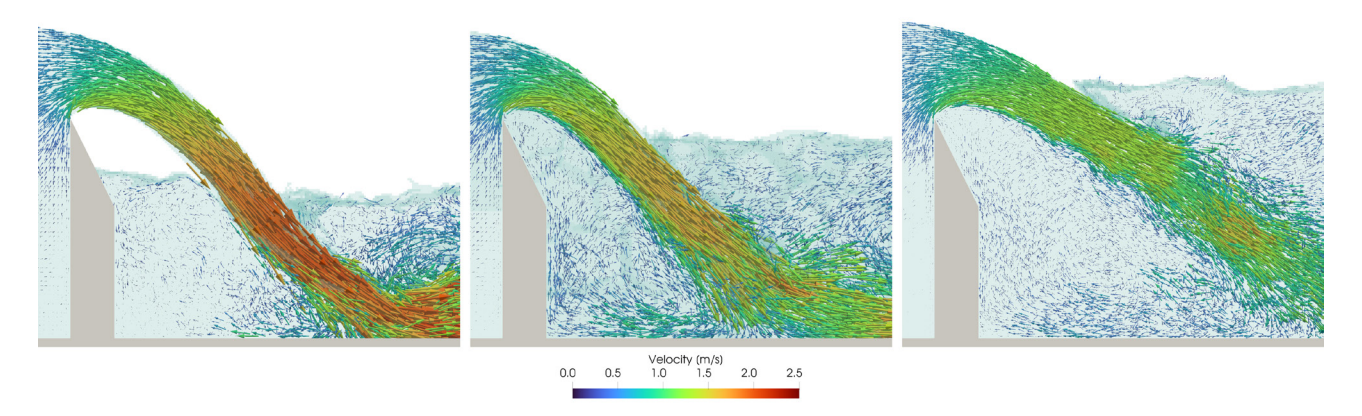


Figure 9: Different situations in the water cushion between nappe and weir. Absolute velocities and directions are shown. The arrows are scaled and coloured according to velocity. The aerated low tailwater level situation (left) shows considerably less rotational movement than the medium (middle) and high tailwater situations (right).

4.1 Collisions

Collisions are often the decisive criterion in the assessment of downstream fish passage over weirs (Pflugrath et al., 2019). Consequently, the accurate representation of such events is of paramount importance. In the numerical model, the number of collisions, potential collisions, and instances of no contact are similar to those in the laboratory model. It is particularly important that the corresponding trends are correctly modelled, with respect to the variation of the tailwater level. This is entirely consistent. It is noteworthy that in both models, although the number of clear collisions increases and the number of particles without contact decreases with increasing tailwater level, the number of possible contacts remains constant. This suggests that even at high tailwater levels, a considerable number of particles are moving in close proximity to the bottom but are not clearly colliding with it. The positions of the collisions are also in good agreement. It is plausible that the observed tendency for collisions to occur at a minimally greater distances from the weir in the numerical model is due to the smaller size of the particles. This results in a slight delay in both the temporal and spatial aspects of the collision. The observations made during the course of the tests also revealed the reason for the initially surprising trend that the collisions occur closest to the weir at medium tailwater levels and farthest away at high tailwater levels. As expected, the collisions tend to move downstream as the water level rises, with a corresponding increase in deflection. However, while the nappe remains aerated at the low water levels, this is no longer the case at the medium water levels. As a result, the nappe is pulled towards the weir body, causing collisions to occur closer to the weir. As the water level continues to rise, this effect is superimposed in the high end sill situation.

Overall, it should be noted that there was no exact agreement between the collisions in the numerical model and the laboratory model. It is not possible to determine an exact number of collisions for fish using this numerical model. On the other hand, the numbers of collisions are of a comparable order of magnitude and there appears to be a strong similarity in principle. The trends are clearly well described. The model is therefore suitable for a comparative assessment of different flow situations.

4.2 Upstream movement

One approach to comparing of particle motion is to consider the occurrence of upstream motion. As this phenomenon has a significant influence on the residence time, this observation is particularly noteworthy. As already described and shown in Figure 9, in the low tailwater situation the rotational motion in the water cushion is notably less pronounced in the numerical model. This also had a noticeable effect on the movement of the particles. In contrast to the laboratory model, where a substantial proportion of particles were observed to enter the water cushion in the low tailwater level scenario, this number was notably lower in the numerical model. However, as this effect is due to drawbacks of the numerical method used, it cannot be attributed to the calculation of the particle movement. Nevertheless, this illustrates the influence of the numerical method, which has the potential to produce unfavourable results. This must be taken into account when analysing the model results. This effect could be reduced by further refinement of the grid in this area.







However, this would not only increase the computational effort, but would also further limit the particle size, as the particles would need to be much smaller than the cells. For both movement patterns, the trend in the numerical model and the laboratory model is consistent. As the tailwater level increases, the number of particles entering the backflow in the water cushion increases whereas the frequency of entering the hydraulic jump is not as affected by the tailwater level.

The evaluation of the distances travelled within the upstream flow confirms the results of the evaluation of the fraction of particles with upstream movement. The distances travelled backwards in the hydraulic jump do not seem to be influenced by the tailwater level, whereas the distances travelled upstream in the water cushion increase with increasing tailwater level. This trend is consistent between the two models. The total distances are also of very similar length, especially in the water cushion.

4.3 Residence time

The residence time is strongly influenced by whether the particles enter a backflow or not. As the proportions of particles that do so are different, it is important to evaluate each group separately. The split analysis again confirms that particles with upstream movement have significantly longer residence times in the stilling basin. When divided into particles with and without upstream movement, the trend is the same for all groups. In the numerical model, the residence time is slightly shorter for particles without upstream movement and longer for particles with upstream movement. As with the collisions and the upstream movement, the numerical model demonstrates an accurate reproduction of the shift in residence times. As the tailwater level rises, the residence times of particles show an increase, regardless of whether they are undergoing upstream motion or not. The similarity in the magnitude of these increases is another indication of the efficacy of the method used.

5 Conclusion

A comparison of the particle movement in a numerical model and a laboratory model was carried out to assess the ability of the numerical method to simulate the passive object transport over weirs. Overall, the results of the different models are of a similar magnitude. The number of collisions was slightly lower in the numerical model than in the laboratory model. In the laboratory model the upstream movements were slightly more frequent, and the residence times were slightly longer. The most notable discrepancy was observed in the number of particles entering the backflow within the water cushion between the weir and the nappe in the low tailwater scenario. This discrepancy can be attributed to a methodological issue inherent to the VoF method and the insufficient grid resolution in the shear zone of the nappe. While the use of an even finer grid could potentially mitigate this problem, it is not a comprehensive solution, as the limitations of VoF cannot be completely eliminated. Overall, it is important to understand and consider the fundamental limitations of numerical methods when using them.

Although the particle motion patterns observed in the two models are not identical, they are nevertheless highly analogous. The resulting data is generally at scale and the overall trends are consistently correctly represented. The method has been demonstrated to be suitable for modelling the passive object transport over the weir. There is also no apparent reason against simulating undershot weirs. In the long term, this method is intended to be used in the context of downstream fish assessment at weirs. Due to simplifications such as ignoring the unique shape and active movement of the fish, the trajectories of individual fish cannot be reproduced with perfect accuracy. It is beyond the capabilities of the method to perfectly determine all fish trajectories and collisions. However, the movement of passive tracers and, in particular, the number of collisions of these tracers, is in principle correctly modelled. Therefore, considering the limitations of the applied numerical method and a sufficient grid resolution to map relevant processes, there is no impediment to the utilisation of the method to assess the downstream fish migration at hydraulic structures without moving parts. The validated method can be used to compare different situations in the context of a qualitative study. It facilitates the assessment of collisions, as well as the evaluation of pressure changes and local velocity gradients experienced by the particles, due to the generally consistent particle trajectories.





Acknowledgements

Author contributions (CRediT)

LK: Conceptualization, Investigation, Methodology, Software, Visualization, Writing – original draft. CT: Conceptualization, Software, Supervision, Writing – review & editing. RW: Conceptualization, Supervision, Writing – review & editing. BL: Supervision, Writing – review & editing.

Use of AI

During the preparation of this work, the authors used ChatGPT and DeepL in order to improve the text in terms of linguistic accuracy and readability. After using these tools, the authors reviewed, edited, made the content their own and validated the outcome as needed, and take full responsibility for the content of the publication.

Data access statement

The data acquired is available from the BAW-Datenrepository database (DOI: https://doi.org/10.48437/99f329-73aee6)

Conflict of interest (COI)

There is no conflict of interest.

Abbreviations

VOF	Volume of Fluid

CFD Computational Fluid Dynamics

BAW Federal Waterways Engineering and Research Institute

DEM Discrete Element Method

ADV Acoustic Doppler Velocimeter

FVM Finite Volume Method

RANS Reynolds-Averaged Navier-Stokes

LES Large Eddy Simulation

References

References

- 3D Systems Inc. (Ed.). DuraForm ProX PA. https://www.3dsystems.com/sites/default/files/2022-02/3d-systems-duraform-prox-pa-sls-datasheet-usen-2022-02-11-a-print.pdf
- Allan, D. B., Caswell, T., Keim, N. C., van der Wel, C. M., & Verweij, R. W. (2024). soft-matter/trackpy: v0.6.2 [Computer software]. Zenodo.
- Argyropoulos, C. D., & Markatos, N. C. (2015). Recent advances on the numerical modelling of turbulent flows. Applied Mathematical Modelling, 39(2), 693–732. https://doi.org/10.1016/j.apm.2014.07.001
- Benigni, H., Schneider, J., Reckendorfer, W., Jaberg, H., Zenz, G., & Tuhtan, J. (2021). Numerical simulation and experimental verification of downstream fish migration in a Kaplan turbine. IOP Conference Series: Earth and Environmental Science, 774(1), 12149. https://doi.org/10.1088/1755-1315/774/1/012149
- Benigni, H., Schneider, J., Reckendorfer, W., Schiffer, J., Tuhtan, J., Leithner, S., Zenz, G., & Meusburger, P. (2022). Numerical simulation and experimental verification of downstream fish migration in a Bulb turbine. IOP Conference Series: Earth and Environmental Science, 1079(1), 12101. https://doi.org/10.1088/1755-1315/1079/1/012101
- Bensing, K., Tuhtan, J. A., Toming, G., Khan, A. H., & Lehmann, B. (2022). Fish body geometry reduces the upstream velocity profile in subcritical flowing waters. *Aquatic Sciences*, 84(3). https://doi.org/10.1007/s00027-022-00863-6
- Brackbill, J., Kothe, D., & Zemach, C. (1992). A continuum method for modeling surface tension. Journal of Computational Physics, 100(2), 335–354. https://doi.org/10.1016/0021-9991(92)90240-Y



- Coutant, C. C., & Whitney, R. R. (2000). Fish Behavior in Relation to Passage through Hydropower Turbines: A Review. Transactions of the American Fisheries Society, 129(2), 351–380. <a href="https://doi.org/10.1577/1548-8659(2000)129<0351:FBIRTP>2.0.CO;2">https://doi.org/10.1577/1548-8659(2000)129<0351:FBIRTP>2.0.CO;2
- Crocker, J. C., & Grier, D. G. (1996). Methods of Digital Video Microscopy for Colloidal Studies. Journal of Colloid and Interface Science, 179(1), 298–310. https://doi.org/10.1006/jcis.1996.0217
- Endress + Hauser Group Services AG (Ed.). Proline Promag 53: Electromagnetic Flow Measuring System. https://portal.endress.com/wa012/CSProxyCache.dll?get&forward=archive.endress.com/sa8080%2Farchive/s3F_&pVersion=0046&contRep=WD&docId=4C1F3A2D6130551DE10000000A35E042&compId=BA054DEN_0610.pdf
- Fernandes, C., Semyonov, D., Ferrás, L. L., & Nóbrega, J. M. (2018). Validation of the CFD-DPM solver DPMFoam in OpenFOAM® through analytical, numerical and experimental comparisons. Granular Matter, 20(4). https://doi.org/10.1007/s10035-018-0834-x
- G.U.N.T. Gerätebau GmbH (2025). HM 163: Versuchsrinne 409x500mm. https://www.gunt.de/images/datasheet/722/HM-163-Versuchsrinne-409x500mm-gunt-722-pdf 1 de-DE.pdf
- Gisen, D. C., Weichert, R. B., & Nestler, J. M. (2017). Optimizing attraction flow for upstream fish passage at a hydropower dam employing 3D Detached-Eddy Simulation. Ecological Engineering, 100, 344–353. https://doi.org/10.1016/j.ecoleng.2016.10.065
- GoPro Inc. (2023). GoPro HERO12 Black Product Manual. https://gopro.my.salesforce.com/sfc/p/#o0000000HJuF/a/8a000000Ahpd/Jat_P5q9uAtmsapajO6peeDTXVYwtGt2dFYnICuhOO4
- Greifzu, F., Kratzsch, C., Forgber, T., Lindner, F., & Schwarze, R. (2016). Assessment of particle-tracking models for dispersed particle-laden flows implemented in OpenFOAM and ANSYS FLUENT. Engineering Applications of Computational Fluid Mechanics, 10(1), 30–43. https://doi.org/10.1080/19942060.2015.1104266
- Hirt, C., & Nichols, B. (1981). Volume of fluid (VOF) method for the dynamics of free boundaries. Journal of Computational Physics, 39(1), 201–225. https://doi.org/10.1016/0021-9991(81)90145-5
- Jasak, H [Hrvoje]. (1996). Error Analysis and Estimation for the Finite Volume Method with Applications to Fluid Flows [PhD Thesis]. Imperial College London, London (United Kingdom).
- Jones, P. E., Svendsen, J. C., Börger, L., Champneys, T., Consuegra, S., Jones, J. A. H., & Garcia de Leaniz, C. (2020). One size does not fit all: Inter- and intraspecific variation in the swimming performance of contrasting freshwater fish. Conservation Physiology, 8(1), coaa126. https://doi.org/10.1093/conphys/coaa126
- Kaminski, L., Thorenz, C., Weichert, R., & Lehmann, B. (2024). Computational fluid dynamics simulation of passive downstream fish passage over a weir with OpenFOAM ®. Journal of Ecohydraulics, 1–24. https://doi.org/10.1080/24705357.2024.2363770
- Li, L., & Li, B. (2018). Implementation and validation of a volume-of-fluid and discrete-element-method combined solver in OpenFOAM. Particuology, 39, 109–115. https://doi.org/10.1016/j.partic.2017.09.007
- Mei, R. (1992). An approximate expression for the shear lift force on a spherical particle at finite reynolds number. International Journal of Multiphase Flow, 18(1), 145–147. https://doi.org/10.1016/0301-9322(92)90012-6
- Naderi Rad, I. (2016). Application of numerical methods in design of hydraulic structures. Communications on Advanced Computational Science with Applications, 2016(1), 1–15. https://doi.org/10.5899/2016/cacsa-00050
- Nortek AS (2018). The Comprehensive Manual for Velocimeters. https://www.nortekgroup.com/assets/software/N3015-030-Comprehensive-Manual-Velocimeters 1118.pdf
- OpenCV.org. (2024). Open Source Computer Vision Library (Version 4.10.0.84) [Computer software]. https://docs.opencv.org/4.10.0/
- Pflugrath, B. D., Boys, C. A., Cathers, B., & Deng, Z. D. (2019). Over or under? Autonomous sensor fish reveals why overshot weirs may be safer than undershot weirs for fish passage. Ecological Engineering, 132, 41–48. https://doi.org/10.1016/j.ecoleng.2019.03.010
- Pope, S. B. (2001). Turbulent Flows. Measurement Science and Technology, 12(11), 2020–2021. https://doi.org/10.1088/0957-0233/12/11/705
- Python Software Foundation. (2024). Python (Version 3.11.9) [Computer software]. https://docs.python.org/3.11/





- Richmond, M. C., Serkowski, J. A., Rakowski, C. L., Graf, M., & Romero-Gomez, P. (2015). Comparative study of barotrauma risk during fish passage through Kaplan turbines. https://doi.org/10.13140/RG.2.1.3747.0321
- Rodi, W. (2017). Turbulence modeling and simulation in hydraulics: A historical review. Journal of Hydraulic Engineering, 143(5), Article 03117001. https://doi.org/10.1061/(ASCE)HY.1943-7900.0001288
- Romero-Gomez, P., Singh, R. K., Richmond, M. C., & Weissenberger, S. (2021). Numerical investigation of inertial sphere impaction on a cylinder in subcritical flow. Particulate Science and Technology, 40(1), 35–49. https://doi.org/10.1080/02726351.2021.1904308
- Romero-Gomez, P., Richmond, M. C. (2017). Movement and collision of Lagrangian particles in hydro-turbine intakes: a case study. Journal of Hydraulic Research, 55(5), 706–720. https://doi.org/10.1080/00221686.2017.1289258
- Romero-Gomez, P., Poomchaivej, T., Razdan, R., Robinson, W., Peyreder, R., Raeder, M., & Baumgartner, L. J. (2024). Sensor Fish Deployments at the Xayaburi Hydropower Plant: Measurements and Simulations. Water, 16(5), 775. https://doi.org/10.3390/w16050775
- Rusche, H. (2003). Computational fluid dynamics of dispersed two-phase flows at high phase fractions. Imperial College London, London (United Kingdom).
- Saffman, P. G. (1965). The lift on a small sphere in a slow shear flow. Journal of Fluid Mechanics, 22(2), 385–400. https://doi.org/10.1017/S0022112065000824
- Schulze, L. (2018). Development of an Application-Oriented Approach for Two-Phase Modelling in Hydraulic Engineering [Doctoral Thesis]. Technische Universität Dresden, Dresden (Germany). https://hdl.handle.net/20.500.11970/105431
- SICK AG (Ed.). Ultraschallsensoren: Vielseitig und präzise messen mit Ultraschallsensoren von Sick. https://cdn.sick.com/media/docs/9/09/709/Product_information_Ultrasonic_Sensors_UM30_UM18_UM12_UC30_UC12_UC4_de_IM0043709.PDF
- Singh, R., Richmond, M., Romero-Gomez, P., Rakowski, C., & Serkowski, J. (2021). Validation of computational fluid dynamics simulations for the biological performance assessment of hydropower generation units (PNNL-30068).
- Sony Corporation (2016). ILCE-6300 45794101 Manual. https://www.sony.com/electronics/support/res/manuals/4579/45794101M.pdf
- Su, G., Villéger, S., & Brosse, S. (2019). Morphological diversity of freshwater fishes differs between realms, but morphologically extreme species are widespread. *Global Ecology and Biogeography*, 28(2), 211–221. https://doi.org/10.1111/geb.12843
- Taylor, N. J., & Rumsey, C. L. (2021). CFD Validation Experiments: Toward a Broader Perspective. In AIAA Scitech 2021 Forum 2021. https://doi.org/10.2514/6.2021-1933
- Thorenz, C., Belzner, F., Hartung, T., & Schulze, L. (2017). Numerische Methoden zur Simulation von Schleusenfüllprozessen. In BAWMitteilungen 100 (91–108.). Bundesanstalt für Wasserbau.
- Ubbink, U. (1997). Numerical prediction of two fluid systems with sharp interfaces [PhD Thesis]. Imperial College London, London (United Kingdom).
- van Os, A., Soulsby, R., & Kirkegaard, J. (2004). The future role of experimental methods in European hydraulic research: towards a balanced methodology. Journal of Hydraulic Research, 42(4), 341–356. https://doi.org/10.1080/00221686.2004.9728401
- Vollmari, K., Jasevičius, R., & Kruggel-Emden, H. (2016). Experimental and numerical study of fluidization and pressure drop of spherical and non-spherical particles in a model scale fluidized bed. Powder Technology, 291, 506–521. https://doi.org/10.1016/j.powtec.2015.11.045
- Wagner, M. (2024). Numerical and Experimental Investigation of a Sharp-Crested Weir Nappe. Karlsruher Institut für Technologie (KIT). https://doi.org/10.5445/IR/1000172539
- Weller, H. G., Tabor, G., Jasak, H [H.], & Fureby, C. (1998). A tensorial approach to computational continuum mechanics using object-oriented techniques. Computers in Physics, 12(6), 620. https://doi.org/10.1063/1.168744
- Yoshizawa, A. (1986). Statistical theory for compressible turbulent shear flows, with the application to subgrid modeling. Physics of Fluids, 29(7), 2152. https://doi.org/10.1063/1.865552